Time-Resolved Changes in Dielectric Constant of Metal Halide Perovskites under Illumination

Journal:	*Journal of the American Chemical Society*
Manuscript ID	ja-2020-073072.R2
Manuscript Type:	Communication
Date Submitted by the Author:	05-Nov-2020
Complete List of Authors:	Hong, Min Ji; Oregon State University, School of Electrical Engineering and Computer Science Zhu, Liangdong; Oregon State University, Department of Chemistry Chen, Cheng; Oregon State University, Department of Chemistry Tang, Longteng; Oregon State University, Department of Chemistry Lin, Yen-Hung; University of Oxford Mathematical Physical and Life Sciences Division, Physics Li, Wen; University of Oxford Mathematical Physical and Life Sciences Division, Physics Johnson, Rose; Oregon State University, School of Chemical, Biological and Environmental Engineering Chattopadhyay, Shirsopratim; Oregon State University, School of Electrical Engineering and Computer Science Snaith, Henry; University of Oxford, Physics Fang, Chong; Oregon State University, Department of Chemistry Labram, John; Oregon State University, School of Electrical Engineering and Computer Science

Time-Resolved Changes in Dielectric Constant of Metal Halide Perovskites under Illumination

Min Ji Hong,[1] Liangdong Zhu,[2] Cheng Chen,[2] Longteng Tang,[2] Yen-Hung Lin,[3] Wen Li,[3,4] Rose Johnson,[5] Shirsopratim Chattopadhyay,[1] Henry J. Snaith,[3] Chong Fang,[2*] John G. Labram[1*]

[1]School of Electrical Engineering and Computer Science, Oregon State University, Corvallis, Oregon 97331, USA
[2]Department of Chemistry, Oregon State University, Corvallis, Oregon 97331, USA
[3]Clarendon Laboratory, Department of Physics, University of Oxford, Parks Road, Oxford OX1 3PU, UK
[4]Institute of Flexible Electronics (IFE), Northwestern Polytechnical University, Xi'an 710072, China
[5]School of Chemical, Biological and Environmental Engineering, Oregon State University, Corvallis, Oregon 97331, USA

ABSTRACT: Despite their impressive performance as a solar absorber, much remains unknown on the fundamental properties of metal halide perovskites (MHPs). Their polar nature in particular is an intense area of study, and the relative permittivity (ε_r) is a parameter widely used to quantify polarization over a range of different timescales. In this report, we have exploited frequency-dependent time-resolved microwave conductivity (TRMC) to study how ε_r of a range of MHPs changes as a function of time, upon optical illumination. Further characterization of charge carriers and polarizability are conducted by femtosecond transient absorption and stimulated Raman spectroscopy. We find that changes in ε_r are roughly proportional to photogenerated carrier density, but decay with a shorter time constant than conductance, suggesting that the presence of charge carriers alone do not determine polarization.

Despite being processable from solution at low temperature (≤ 100°C),[1] lab-scale solar cells based on metal halide perovskites (MHPs) exhibit certified power conversion efficiencies (PCEs) comparable to those of monocrystalline silicon.[2] While MHPs offer industry and the academic community many exciting opportunities, consistent mechanistic understanding and consensus still lag behind more established systems such as organic semiconductors[3] or silicon,[4] with many unanswered questions remaining.[5]

Ionic semiconductors have long been known to exhibit properties distinct from covalent semiconductors,[6] and the polar nature of MHPs is an intense area of study.[7–10] The relative permittivity (ε_r) is a parameter widely-used to encapsulate polarization over a range of different timescales.[10,11] As expected for an ionic system, the relative permittivity in MHPs is comparatively large ($\varepsilon_r \sim 5-50$)[10] when likened to a covalent system, and depends heavily on temperature.[12] A so-called giant dielectric constant has been reported in MHPs, where ε_r increases by three orders of magnitude under illumination from 1 sun conditions, at low probe frequencies.[13] This large dielectric constant has been invoked to explain some of the prominent unresolved issues in the theory of MHPs, such as large polarons, enhanced screening, and defect tolerance.[14–17]

In this report we use the contactless semiconductor characterization technique, time-resolved microwave conductivity (TRMC),[18,19] to evaluate photoinduced changes in the real component of relative permittivity ($\Delta\varepsilon_r$) as a function of time. TRMC is traditionally employed to evaluate photoinduced changes in the conductance (ΔG) of thin films,[18] crystals,[20] fluids,[21] suspensions,[22] powders,[23] or discontinuous films.[24] Cavity-based TRMC additionally enables one to probe photoinduced changes in the dielectric constant ($\Delta\varepsilon_r$), through changes in resonant frequency.[25–30] Typically the community casts changes in the real component of dielectric constant into the imaginary component ($\Delta G''$) of complex conductance,[28] and interpret it in this context. For simplicity we here just evaluate and consider $\Delta\varepsilon_r$. While impedance spectroscopy is the standard technique for evaluating ε_r in photovoltaic materials for frequencies up to ~MHz,[31] cavity-based TRMC enables one to probe ε_r in the traditionally challenging[11] regime of ~10 GHz.[32] Because TRMC is designed to study the electrical properties as a function of time, t, with close to nanosecond resolution, it allows one to evaluate $\Delta\varepsilon_r(t)$, in response to optical stimulation, with similar resolution. TRMC does not require electrical contacts, and hence can eliminate potential ambiguity arising from interfacial phenomena.[33]

In this work, we examine two mixed-cation, mixed-halide perovskite compositions: a double-cation composition: $FA_{0.83}Cs_{0.17}Pb(I_{0.9}Br_{0.1})_3$ (FACs) and a triple-cation composition: $(FA_{0.83}MA_{0.17})_{0.95}Cs_{0.05}Pb(I_{0.9}Br_{0.1})_3$ (FAMACs), where FA is formamidinium and MA is methylammonium. These compounds are chosen as they are known to lead to high PCE when employed in solar cells,[34,35] and have been shown to be highly stable in air.[36,37] **Figure 1** shows as-measured changes in the real components of conductance (ΔG) and relative permittivity ($\Delta\varepsilon_r$) of these compounds as a function of time before, during, and after illumination by a nanosecond pulsed laser. Similar data are shown for methylammonium lead iodide ($MAPbI_3$), formamidinium lead iodide ($FAPbI_3$), lead iodide (PbI_2), and the organic semiconductor blend of poly(3-hexylthiophene-2,5-diyl) and phenyl-C_{61}-butyric acid methyl ester (P3HT:$PC_{61}BM$), in the Supporting Information Figure S1.

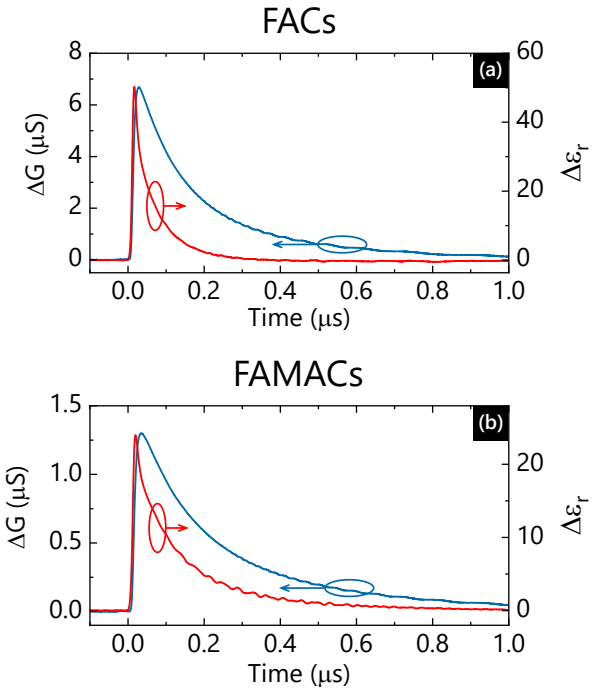

Figure 1 Change in the real component of conductance (left axis, blue line) and relative permittivity (right axis, red line) of (a) FACs and (b) FAMACs, measured as a function of time, before, during, and after illumination by a 532 nm, nanosecond pulsed laser. Incident laser fluence was ~6 × 10^{13} cm^{-2} in all cases.

A detailed description of how these parameters were extracted is provided in Supporting Information Section S2, but the technique relies on evaluating changes in the resonant frequency of microwave cavity as a result of optical stimulation. Signals where the peak width is comparable to the response time of our cavity, which is roughly 5 ns, can be interpreted as artefacts of the technique (see Supporting Information Section S4 for more details). We hence conclude that $MAPbI_3$, $FAPbI_3$, PbI_2, and P3HT:$PC_{61}BM$, exhibit no measurable $\Delta\varepsilon_r$. The mixed-halide, mixed-cation MHP compounds, however, exhibit a non-negligible $\Delta\varepsilon_r$.

While the peak values of ΔG reported here are lower than those reported elsewhere in the literature,[38] relative values are generally unambiguous. A number of instrumental and analytical factors are known to affect these extracted values.[19] It is also important to point out that, while all samples were fabricated, transported, and stored in an inert environment, all TRMC measurements were carried out in air. In Section S5 of the Supporting Information we measured ΔG as we flowed N_2 over $MAPbI_3$ and $FAPbI_3$ samples, and under atmospheric-pressure air. For these short-duration experiments we did not observe appreciable differences in transport behavior in N_2 compared to air. We however are aware that over long periods of time, exposure to air can significantly affect the properties of MHPs.[39]

By carrying out a similar analysis as a function of incident laser fluence, we can approximate how $\Delta\varepsilon_r$ depends on the carrier concentration (see Supporting Information Section S6 for more details). **Figure 2** shows the peak value of $\Delta\varepsilon_r$ as a function of the approximate carrier density in FACs and FAMACs.

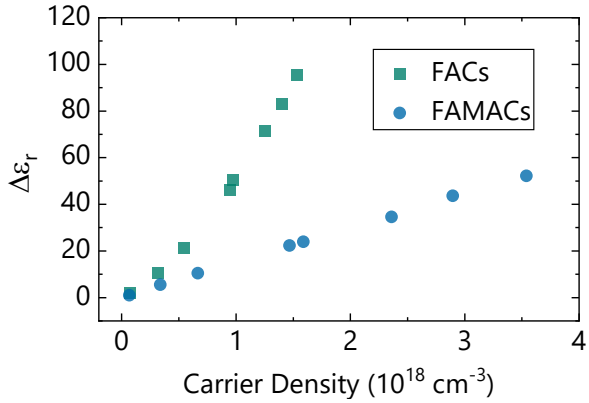

Figure 2 Photoinduced change in the real component of relative permittivity as a function of approximate charge carrier density of FACs and FAMACs.

The origin of the imaginary component of conductance, and the relative magnitude of $\Delta G''$ to ΔG, remains under debate. Field-induced time resolved microwave conductivity (FI-TRMC)[40,41] has been used to study the nature of charge transport in a range of systems including organic semiconductors[29] and graphene[42] by studying complex conductance. Changes in $\Delta G''$ (and implicitly $\Delta\varepsilon_r$) observed in thin films of TiO_2 upon illumination have been associated with trap states,[28] invoking Drude[43] and Drude-Smith[44] models to describe the motion of charge carriers in this system. Similar studies into MHPs, however, present a more complicated picture where the molecular motions of A-site cations and polaronic charges contribute to $\Delta G''$.[25]

The frequency regime we probe in these experiments (~10 GHz) is associated with molecular motions of A-site cations.[32,45] In a previous report we illustrated how the addition of a piperidinium-salt 1-butyl-1-methylpiperidinium tetrafluoroborate ($[BMP]^+[BF_4]^-$) can reduce trap density in FACs films, without significantly modifying the long-range charge carrier mobility.[46] Here we measured $\Delta\varepsilon_r$ against carrier concentration for thin films of FACs with and without the $[BMP]^+[BF_4]^-$ additive (see Supporting Information Figure S8). While we observed a small change in $\Delta\varepsilon_r$ as a function of carrier density with and without the additive, we do not consider this difference in $\Delta\varepsilon_r$ large enough to be explained by the reduction in the concentration of trap states alone. The difference is much smaller than that exhibited between FACs and FAMACs in **Figure 2**, which are anticipated to have similar trap density. For this reason, $\Delta\varepsilon_r$ is here primarily attributed to photoinduced changes in the A-site cation motions, although we acknowledge a number of sources for $\Delta G''$ are possible.

To ensure that there were no systematic changes in measurement or sample conditions over the duration of the experiment, pristine FACs was measured in opposite sweeping directions. The extracted change in $\Delta\varepsilon_r$ versus carrier density (see Supporting Information Figure S9) shows only small differences between forward and reverse sweeps.

From our transient data we can evaluate the half-life $\tau_{1/2}$, defined as the time taken for ΔG or $\Delta\varepsilon_r$ to reach half of its peak value.[28,47] **Figure 3** shows $\tau_{1/2}$ extracted as a function of laser fluence for ΔG and $\Delta\varepsilon_r$, for FACs and FAMACs. The values of $\tau_{1/2}$ were evaluated from measured transient data, which was

deconvolved with the instrument response function[18] of the apparatus.

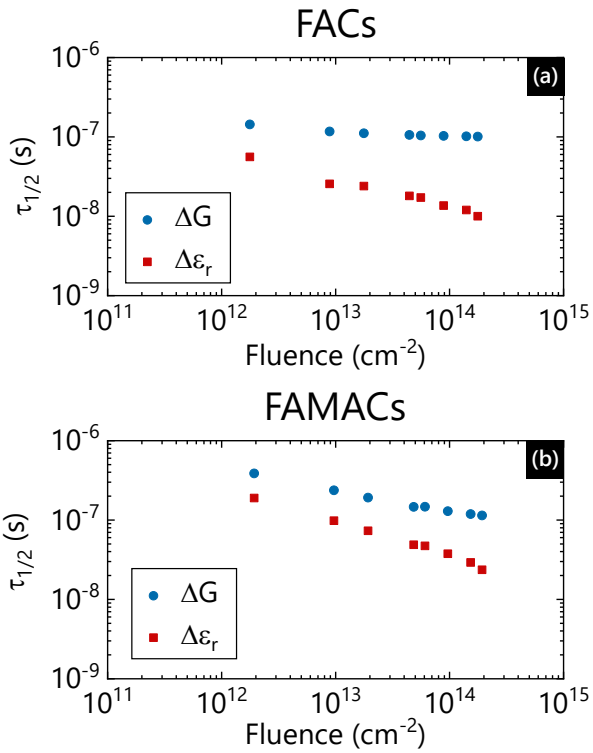

Figure 3 Half-life $\tau_{1/2}$ of photoconductance (ΔG) and change in relative permittivity ($\Delta\varepsilon_r$) as a function of fluence for FACs and FAMACs.

Figure 3 shows that $\Delta\varepsilon_r$ decays over a different timescale from ΔG for both the FACs and FAMACs samples. This suggests that, while they are clearly correlated changes (see **Figure 2**), the relative permittivity is not simply due to the presence of charge carriers alone. It is important to emphasize here that ΔG and $\Delta\varepsilon_r$ have been evaluated from different fit parameters of the same data, meaning that differences in measurement or sample conditions are not responsible.

To help probe the underlying electronic and vibrational features on molecular timescales we employed femtosecond transient absorption (fs-TA) and ground-state femtosecond stimulated Raman spectroscopy (GS-FSRS)[48,49] on FACs and FAMACs thin-film samples (see Supporting Information Section S9 for details). We tuned the 530 nm photoexcitation pulse energy from 0.01 to 0.15 μJ and collected the fs-TA spectra. Higher pump power corresponds to higher carrier density in a similar range of **Figure 2**, leading to the lengthening of the photobleaching band recovery time due to the commonly invoked "phonon bottleneck" to cool down hot charge carriers up to hundreds of picoseconds timescale (see Supporting Information Section S9 for further discussions).[50,51] Using global analysis of the fs-TA spectra (see the retrieved lifetimes in Table S3 and evolution-associated difference spectra in Figure S10), we uncovered the time constant (k^{-1}) that is most sensitive to the laser fluence, and plotted the corresponding rate constants for FACs and FAMACs in **Figure 4(a)**. By assuming that carrier thermalization is primarily due to electron-longitudinal optical (LO) phonon scattering we would expect k to decrease with increasing ε_r, as described by the electron-phonon scattering equation (see Section S9).[50,52] This is consistent with our TRMC data.

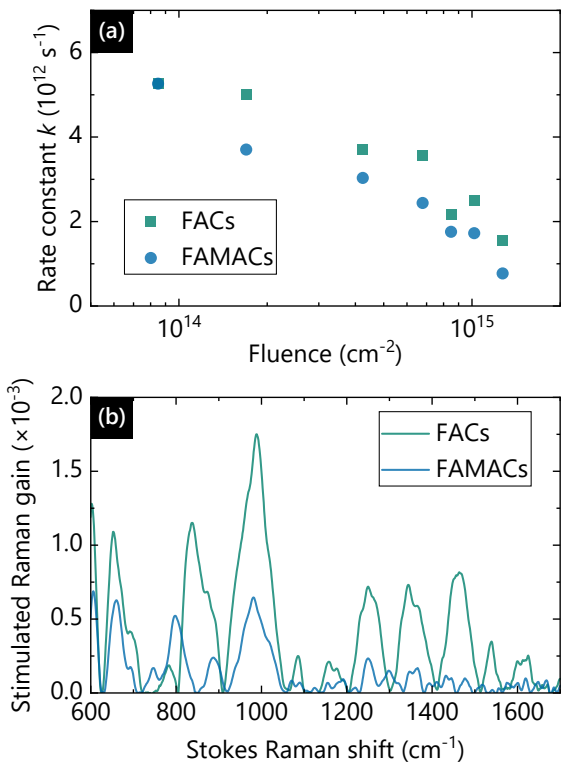

Figure 4 Electronic and vibrational spectroscopic characterization of FACs and FAMACs with ultrafast laser pulses. (a) The second decay rate constant from global analysis of the femtosecond transient absorption spectra of FACs and FAMACs as a function of fluence. The femtosecond pump wavelength is 530 nm. (b) Ground-state femtosecond stimulated Raman spectroscopy (FSRS) of FACs and FAMACs. The picosecond Raman pump is at 800 nm and the femtosecond Raman probe is on the Stokes side.

Notably, GS-FSRS in **Figure 4(b)** manifests larger peak intensities for FACs than FAMACs under similar pre-resonance conditions (Raman pump at 800 nm with 0.4 μJ pulse energy, to the red side of the electronic absorption cutoff wavelength around 750 nm). This result reveals that the A-site organic cations likely have larger electric polarizabilities (hence the Raman peak intensities,[9,53] e.g., ~1000 cm^{-1} peak attributed to the C–N stretch) in FACs than FAMACs. In other words, it can be concluded that the presence of a small amount of MA effectively reduces the polarizability of MHPs.

In conclusion, using frequency-dependent TRMC, we have studied how the ~10 GHz dielectric constant (ε_r) of mixed-halide, mixed-cation MHPs exhibit notable changes under illumination. The changes in ε_r are roughly proportional to photogenerated carrier density, corroborated by the pump-dependent fs-TA experiments. Interestingly, the timescales involved in such changes in conductance are distinct from those associated with changes in ε_r. The dynamics of molecular cations were further characterized by vibration-sensitive FSRS measurements, revealing a larger polarizability of FACs than FAMACs, and suggesting that a small amount of MA effectively reduces the polarizability of MHPs. The correlated TRMC and ultrafast spec-

troscopic results reported in this work could help the community better understand the relationships between optical illumination and polarizability in this class of materials.

ASSOCIATED CONTENT

The Supporting Information is available free of charge at https://pubs.acs.org/doi/xxx.

Experimental methods, analysis technique for frequency-dependent time-resolved microwave conductivity (TRMC), cavity response time, deconvolution of TRMC signals, measurements under nitrogen, evaluation of carrier density, TRMC data of the additive-treated sample, analysis of measurement-to-measurement variation, and fs-TA spectroscopy with global analysis.

AUTHOR INFORMATION

Corresponding Authors

* John G. Labram - *School of Electrical Engineering and Computer Science, Oregon State University, Corvallis, Oregon 97331, USA.* http://orcid.org/0000-0001-6562-9895. Email: john.labram@oregonstate.edu.

* Chong Fang - *Department of Chemistry, Oregon State University, Corvallis, Oregon 97331, USA.* https://orcid.org/0000-0002-8879-1825. Email: chong.fang@oregonstate.edu.

Notes

The authors declare no competing interests.

ACKNOWLEDGMENTS

M.J.H. and J.G.L. thank the NSF for financial support (ECCS-1942558). The ultrafast laser spectroscopic setups are supported by the NSF CAREER grant to C.F. (CHE-1455353), with additional lab personnel support provided by the NSF MRI grant (DMR-1920368).

REFERENCES

(1) Burschka, J.; Pellet, N.; Moon, S.-J.; Humphry-Baker, R.; Gao, P.; Nazeeruddin, M. K.; Gratzel, M. Sequential Deposition as a Route to High-Performance Perovskite-Sensitized Solar Cells. *Nature* **2013**, *499* (7458), 316–319.

(2) Green, M. A.; Dunlop, E. D.; Levi, D. H.; Hohl-Ebinger, J.; Yoshita, M.; Ho-Baillie, A. W. Y. Solar Cell Efficiency Tables (Version 54). *Progress in Photovoltaics: Research and Applications* **2019**, *27* (7), 565–575. https://doi.org/10.1002/pip.3171.

(3) Nelson, J. Polymer:Fullerene Bulk Heterojunction Solar Cells. *Materials Today* **2011**, *14* (10), 462–470. https://doi.org/10.1016/S1369-7021(11)70210-3.

(4) Battaglia, C.; Cuevas, A.; De Wolf, S. High-Efficiency Crystalline Silicon Solar Cells: Status and Perspectives. *Energy Environ. Sci.* **2016**, *9* (5), 1552–1576. https://doi.org/10.1039/C5EE03380B.

(5) Egger, D. A.; Bera, A.; Cahen, D.; Hodes, G.; Kirchartz, T.; Kronik, L.; Lovrincic, R.; Rappe, A. M.; Reichman, D. R.; Yaffe, O. What Remains Unexplained about the Properties of Halide Perovskites? *Advanced Materials* **2018**, *30* (20), 1800691. https://doi.org/10.1002/adma.201800691.

(6) Kurtin, S.; McGill, T. C.; Mead, C. A. Fundamental Transition in the Electronic Nature of Solids. *Phys. Rev. Lett.* **1969**, *22* (26), 1433–1436. https://doi.org/10.1103/PhysRevLett.22.1433.

(7) Frost, J. M.; Butler, K. T.; Brivio, F.; Hendon, C. H.; van Schilfgaarde, M.; Walsh, A. Atomistic Origins of High-Performance in Hybrid Halide Perovskite Solar Cells. *Nano Letters* **2014**, *14* (5), 2584–2590. https://doi.org/10.1021/nl500390f.

(8) Eames, C.; Frost, J. M.; Barnes, P. R. F.; O'Regan, B. C.; Walsh, A.; Islam, M. S. Ionic Transport in Hybrid Lead Iodide Perovskite Solar Cells. *Nat Commun* **2015**, *6*, 7497. https://doi.org/10.1038/ncomms8497.

(9) Frost, J. M.; Walsh, A. What Is Moving in Hybrid Halide Perovskite Solar Cells? *Accounts of Chemical Research* **2016**, *49* (3), 528–535. https://doi.org/10.1021/acs.accounts.5b00431.

(10) Wilson, J. N.; Frost, J. M.; Wallace, S. K.; Walsh, A. Dielectric and Ferroic Properties of Metal Halide Perovskites. *APL Materials* **2019**, *7* (1), 010901. https://doi.org/10.1063/1.5079633.

(11) Anusca, I.; Balčiūnas, S.; Gemeiner, P.; Svirskas, Š.; Sanlialp, M.; Lackner, G.; Fettkenhauer, C.; Belovickis, J.; Samulionis, V.; Ivanov, M.; Dkhil, B.; Banys, J.; Shvartsman, V. V.; Lupascu, D. C. Dielectric Response: Answer to Many Questions in the Methylammonium Lead Halide Solar Cell Absorbers. *Advanced Energy Materials* **2017**, *7* (19), 1700600. https://doi.org/10.1002/aenm.201700600.

(12) Onoda-Yamamuro, N.; Matsuo, T.; Suga, H. Dielectric Study of $CH_3NH_3PbX_3$ (X = Cl, Br, I). *Journal of Physics and Chemistry of Solids* **1992**, *53* (7), 935–939. https://doi.org/10.1016/0022-3697(92)90121-S.

(13) Juarez-Perez, E. J.; Sanchez, R. S.; Badia, L.; Garcia-Belmonte, G.; Kang, Y. S.; Mora-Sero, I.; Bisquert, J. Photoinduced Giant Dielectric Constant in Lead Halide Perovskite Solar Cells. *J. Phys. Chem. Lett.* **2014**, *5* (13), 2390–2394. https://doi.org/10.1021/jz5011169.

(14) Zhu, X.-Y.; Podzorov, V. Charge Carriers in Hybrid Organic–Inorganic Lead Halide Perovskites Might Be Protected as Large Polarons. *The Journal of Physical Chemistry Letters* **2015**, *6* (23), 4758–4761. https://doi.org/10.1021/acs.jpclett.5b02462.

(15) Zhu, H.; Miyata, K.; Fu, Y.; Wang, J.; Joshi, P. P.; Niesner, D.; Williams, K. W.; Jin, S.; Zhu, X.-Y. Screening in Crystalline Liquids Protects Energetic Carriers in Hybrid Perovskites. *Science* **2016**, *353* (6306), 1409. https://doi.org/10.1126/science.aaf9570.

(16) Miyata, K.; Meggiolaro, D.; Trinh, M. T.; Joshi, P. P.; Mosconi, E.; Jones, S. C.; Angelis, F. D.; Zhu, X.-Y. Large Polarons in Lead Halide Perovskites. *Science Advances* **2017**, *3* (8), e1701217. https://doi.org/10.1126/sciadv.1701217.

(17) Frost, J. M. Calculating Polaron Mobility in Halide Perovskites. *Phys. Rev. B* **2017**, *96* (19), 195202. https://doi.org/10.1103/PhysRevB.96.195202.

(18) Savenije, T. J.; Ferguson, A. J.; Kopidakis, N.; Rumbles, G. Revealing the Dynamics of Charge Carriers in Polymer:Fullerene Blends Using Photoinduced Time-Re-

solved Microwave Conductivity. *The Journal of Physical Chemistry C* **2013**, *117* (46), 24085–24103. https://doi.org/10.1021/jp406706u.

(19) Reid, O. G.; Moore, D. T.; Li, Z.; Zhao, D.; Yan, Y.; Zhu, K.; Rumbles, G. Quantitative Analysis of Time-Resolved Microwave Conductivity Data. *J. Phys. D: Appl. Phys.* **2017**, *50* (49), 493002. https://doi.org/10.1088/1361-6463/aa9559.

(20) Saeki, A.; Seki, S.; Takenobu, T.; Iwasa, Y.; Tagawa, S. Mobility and Dynamics of Charge Carriers in Rubrene Single Crystals Studied by Flash-Photolysis Microwave Conductivity and Optical Spectroscopy. *Advanced Materials* **2008**, *20* (5), 920–923. https://doi.org/10.1002/adma.200702463.

(21) Warman, J. M.; de Haas, M. P.; Hummel, A. The Detection of Electrons in Pulse Irradiated Liquid Hydrocarbons by Microwave Absorption. *Chem. Phys. Lett.* **1973**, *22* (3), 480-483. https://doi.org/10.1016/0009-2614(73)87012-5.

(22) Warman, J. M.; Haas, M. P. de; Grätzel, M.; Infelta, P. P. Microwave Probing of Electronic Processes in Small Particle Suspensions. *Nature* **1984**, *310* (5975), 306–308. https://doi.org/10.1038/310306a0.

(23) de Haas, M. P.; Warman, J. M.; Anthopoulos, T. D.; de Leeuw, D. M. The Mobility and Decay Kinetics of Charge Carriers in Pulse-Ionized Microcrystalline PCBM Powder. *Advanced Functional Materials* **2006**, *16* (17), 2274–2280. https://doi.org/10.1002/adfm.200500882.

(24) Labram, J. G.; Venkatesan, N. R.; Takacs, C. J.; Evans, H. A.; Perry, E. E.; Wudl, F.; Chabinyc, M. L. Charge Transport in a Two-Dimensional Hybrid Metal Halide Thiocyanate Compound. *Journal of Materials Chemistry C* **2017**, *5* (24), 5930–5938. https://doi.org/10.1039/C7TC01161J.

(25) Yamada, K.; Nishikubo, R.; Oga, H.; Ogomi, Y.; Hayase, S.; Kanno, S.; Imamura, Y.; Hada, M.; Saeki, A. Anomalous Dielectric Behavior of a Pb/Sn Perovskite: Effect of Trapped Charges on Complex Photoconductivity. *ACS Photonics* **2018**, *5* (8), 3189–3197. https://doi.org/10.1021/acsphotonics.8b00422.

(26) Saeki, A.; Seki, S.; Sunagawa, T.; Ushida, K.; Tagawa, S. Charge-Carrier Dynamics in Polythiophene Films Studied by in-Situ Measurement of Flash-Photolysis Time-Resolved Microwave Conductivity (FP-TRMC) and Transient Optical Spectroscopy (TOS). *Philosophical Magazine* **2006**, *86* (9), 1261–1276. https://doi.org/10.1080/14786430500380159.

(27) Fravventura, M. C.; Deligiannis, D.; Schins, J. M.; Siebbeles, L. D. A.; Savenije, T. J. What Limits Photoconductance in Anatase TiO_2 Nanostructures? A Real and Imaginary Microwave Conductance Study. *J. Phys. Chem. C* **2013**, *117* (16), 8032–8040. https://doi.org/10.1021/jp400222t.

(28) Saeki, A.; Yasutani, Y.; Oga, H.; Seki, S. Frequency-Modulated Gigahertz Complex Conductivity of TiO_2 Nanoparticles: Interplay of Free and Shallowly Trapped Electrons. *J. Phys. Chem. C* **2014**, *118* (39), 22561–22572. https://doi.org/10.1021/jp505214d.

(29) Choi, W.; Tsutsui, Y.; Sakurai, T.; Seki, S. Complex Permittivity Analysis Revisited: Microwave Spectroscopy of Organic Semiconductors with Resonant Cavity. *Appl. Phys. Lett.* **2017**, *110* (15), 153303. https://doi.org/10.1063/1.4980078.

(30) Yamada, K.; Suzuki, H.; Abe, R.; Saeki, A. Complex Photoconductivity Reveals How the Nonstoichiometric Sr/Ti Affects the Charge Dynamics of a $SrTiO_3$ Photocatalyst. *J. Phys. Chem. Lett.* **2019**, *10* (8), 1986–1991. https://doi.org/10.1021/acs.jpclett.9b00880.

(31) von Hauff, E. Impedance Spectroscopy for Emerging Photovoltaics. *J. Phys. Chem. C* **2019**, *123* (18), 11329–11346. https://doi.org/10.1021/acs.jpcc.9b00892.

(32) Caselli, V. M.; Fischer, M.; Meggiolaro, D.; Mosconi, E.; De Angelis, F.; Stranks, S. D.; Baumann, A.; Dyakonov, V.; Hutter, E. M.; Savenije, T. J. Charge Carriers Are Not Affected by the Relatively Slow-Rotating Methylammonium Cations in Lead Halide Perovskite Thin Films. *J. Phys. Chem. Lett.* **2019**, *10* (17), 5128–5134. https://doi.org/10.1021/acs.jpclett.9b02160.

(33) Schulz, P.; Cahen, D.; Kahn, A. Halide Perovskites: Is It All about the Interfaces? *Chem. Rev.* **2019**, *119* (5), 3349–3417. https://doi.org/10.1021/acs.chemrev.8b00558.

(34) Saliba, M.; Matsui, T.; Seo, J.-Y.; Domanski, K.; Correa-Baena, J.-P.; Nazeeruddin, M. K.; Zakeeruddin, S. M.; Tress, W.; Abate, A.; Hagfeldt, A.; Grätzel, M. Cesium-Containing Triple Cation Perovskite Solar Cells: Improved Stability, Reproducibility and High Efficiency. *Energy Environ. Sci.* **2016**, *9* (6), 1989–1997. https://doi.org/10.1039/C5EE03874J.

(35) Stolterfoht, M.; Wolff, C. M.; Márquez, J. A.; Zhang, S.; Hages, C. J.; Rothhardt, D.; Albrecht, S.; Burn, P. L.; Meredith, P.; Unold, T.; Neher, D. Visualization and Suppression of Interfacial Recombination for High-Efficiency Large-Area Pin Perovskite Solar Cells. *Nature Energy* **2018**, *3* (10), 847. https://doi.org/10.1038/s41560-018-0219-8.

(36) McMeekin, D. P.; Sadoughi, G.; Rehman, W.; Eperon, G. E.; Saliba, M.; Hörantner, M. T.; Haghighirad, A.; Sakai, N.; Korte, L.; Rech, B.; Johnston, M. B.; Herz, L. M.; Snaith, H. J. A Mixed-Cation Lead Mixed-Halide Perovskite Absorber for Tandem Solar Cells. *Science* **2016**, *351* (6269), 151. https://doi.org/10.1126/science.aad5845.

(37) Turren-Cruz, S.-H.; Hagfeldt, A.; Saliba, M. Methylammonium-Free, High-Performance, and Stable Perovskite Solar Cells on a Planar Architecture. *Science* **2018**, *362* (6413), 449–453. https://doi.org/10.1126/science.aat3583.

(38) Herz, L. M. Charge-Carrier Mobilities in Metal Halide Perovskites: Fundamental Mechanisms and Limits. *ACS Energy Lett.* **2017**, 1539–1548. https://doi.org/10.1021/acsenergylett.7b00276.

(39) Boyd, C. C.; Cheacharoen, R.; Leijtens, T.; McGehee, M. D. Understanding Degradation Mechanisms and Improving Stability of Perovskite Photovoltaics. *Chem. Rev.* **2019**, *119* (5), 3418–3451. https://doi.org/10.1021/acs.chemrev.8b00336.

(40) Honsho, Y.; Miyakai, T.; Sakurai, T.; Saeki, A.; Seki, S. Evaluation of Intrinsic Charge Carrier Transport at Insulator-Semiconductor Interfaces Probed by a Non-Contact Microwave-Based Technique. *Scientific Reports* **2013**, *3*, 3182. https://doi.org/10.1038/srep03182.

(41) Choi, W.; Inoue, J.; Tsutsui, Y.; Sakurai, T.; Seki, S. In-Situ Analysis of Microwave Conductivity and Impedance Spectroscopy for Evaluation of Charge Carrier Dynamics at Interfaces. *Appl. Phys. Lett.* **2017**, *111* (20), 203302. https://doi.org/10.1063/1.5003207.

(42) Choi, W.; Nishiyama, H.; Ogawa, Y.; Ueno, Y.; Furukawa, K.; Takeuchi, T.; Tsutsui, Y.; Sakurai, T.; Seki, S. Relaxation of Plasma Carriers in Graphene: An Approach by Frequency-Dependent Optical Conductivity Measurement. *Advanced Optical Materials* **2018**, *6* (14), 1701402. https://doi.org/10.1002/adom.201701402.

(43) Dunn, H. K.; Peter, L. M.; Bingham, S. J.; Maluta, E.; Walker, A. B. In Situ Detection of Free and Trapped Electrons in Dye-Sensitized Solar Cells by Photo-Induced Microwave Reflectance Measurements. *J. Phys. Chem. C* **2012**, *116* (41), 22063–22072. https://doi.org/10.1021/jp3072074.

(44) Turner, G. M.; Beard, M. C.; Schmuttenmaer, C. A. Carrier Localization and Cooling in Dye-Sensitized Nanocrystalline Titanium Dioxide. *J. Phys. Chem. B* **2002**, *106* (45), 11716–11719. https://doi.org/10.1021/jp025844e.

(45) Poglitsch, A.; Weber, D. Dynamic Disorder in Methylammoniumtrihalogenoplumbates (II) Observed by Millimeter-wave Spectroscopy. *J. Chem. Phys.* **1987**, *87* (11), 6373–6378. https://doi.org/10.1063/1.453467.

(46) Lin, Y.-H.; Sakai, N.; Da, P.; Wu, J.; Sansom, H. C.; Ramadan, A. J.; Mahesh, S.; Liu, J.; Oliver, R. D. J.; Lim, J.; Aspitarte, L.; Sharma, K.; Madhu, P. K.; Morales-Vilches, A. B.; Nayak, P. K.; Bai, S.; Gao, F.; Grovenor, C. R. M.; Johnston, M. B.; Labram, J. G.; Durrant, J. R.; Ball, J. M.; Wenger, B.; Stannowski, B.; Snaith, H. J. A Piperidinium Salt Stabilizes Efficient Metal-Halide Perovskite Solar Cells. *Science* **2020**, *369* (6499), 96–102. https://doi.org/10.1126/science.aba1628.

(47) Oga, H.; Saeki, A.; Ogomi, Y.; Hayase, S.; Seki, S. Improved Understanding of the Electronic and Energetic Landscapes of Perovskite Solar Cells: High Local Charge Carrier Mobility, Reduced Recombination, and Extremely Shallow Traps. *J. Am. Chem. Soc.* **2014**, *136* (39), 13818–13825. https://doi.org/10.1021/ja506936f.

(48) Liu, W.; Wang, Y.; Tang, L.; Oscar, B. G.; Zhu, L.; Fang, C. Panoramic Portrait of Primary Molecular Events Preceding Excited State Proton Transfer in Water. *Chem. Sci.* **2016**, *7* (8), 5484–5494. https://doi.org/10.1039/C6SC00672H.

(49) Fang, C.; Tang, L.; Oscar, B. G.; Chen, C. Capturing Structural Snapshots during Photochemical Reactions with Ultrafast Raman Spectroscopy: From Materials Transformation to Biosensor Responses. *J. Phys. Chem. Lett.* **2018**, *9* (12), 3253–3263. https://doi.org/10.1021/acs.jpclett.8b00373.

(50) Yang, Y.; Ostrowski, D. P.; France, R. M.; Zhu, K.; van de Lagemaat, J.; Luther, J. M.; Beard, M. C. Observation of a Hot-Phonon Bottleneck in Lead-Iodide Perovskites. *Nature Photonics* **2016**, *10* (1), 53–59. https://doi.org/10.1038/nphoton.2015.213.

(51) Zhai, Y.; Sheng, C. X.; Zhang, C.; Vardeny, Z. V. Ultrafast Spectroscopy of Photoexcitations in Organometal Trihalide Perovskites. *Advanced Functional Materials* **2016**, *26* (10), 1617–1627. https://doi.org/10.1002/adfm.201505115.

(52) Ridley, B. K. Hot Phonons in High-Field Transport. *Semiconductor Science and Technology* **1989**, *4* (12), 1142–1150. https://doi.org/10.1088/0268-1242/4/12/016.

(53) Dietze, D. R.; Mathies, R. A. Femtosecond Stimulated Raman Spectroscopy. *ChemPhysChem* **2016**, *17* (9), 1224–1251. https://doi.org/10.1002/cphc.201600104.

Insert Table of Contents artwork here

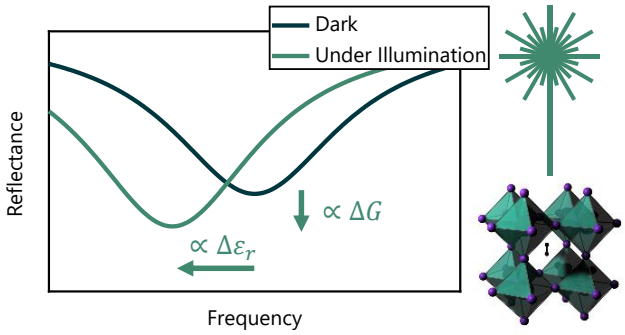

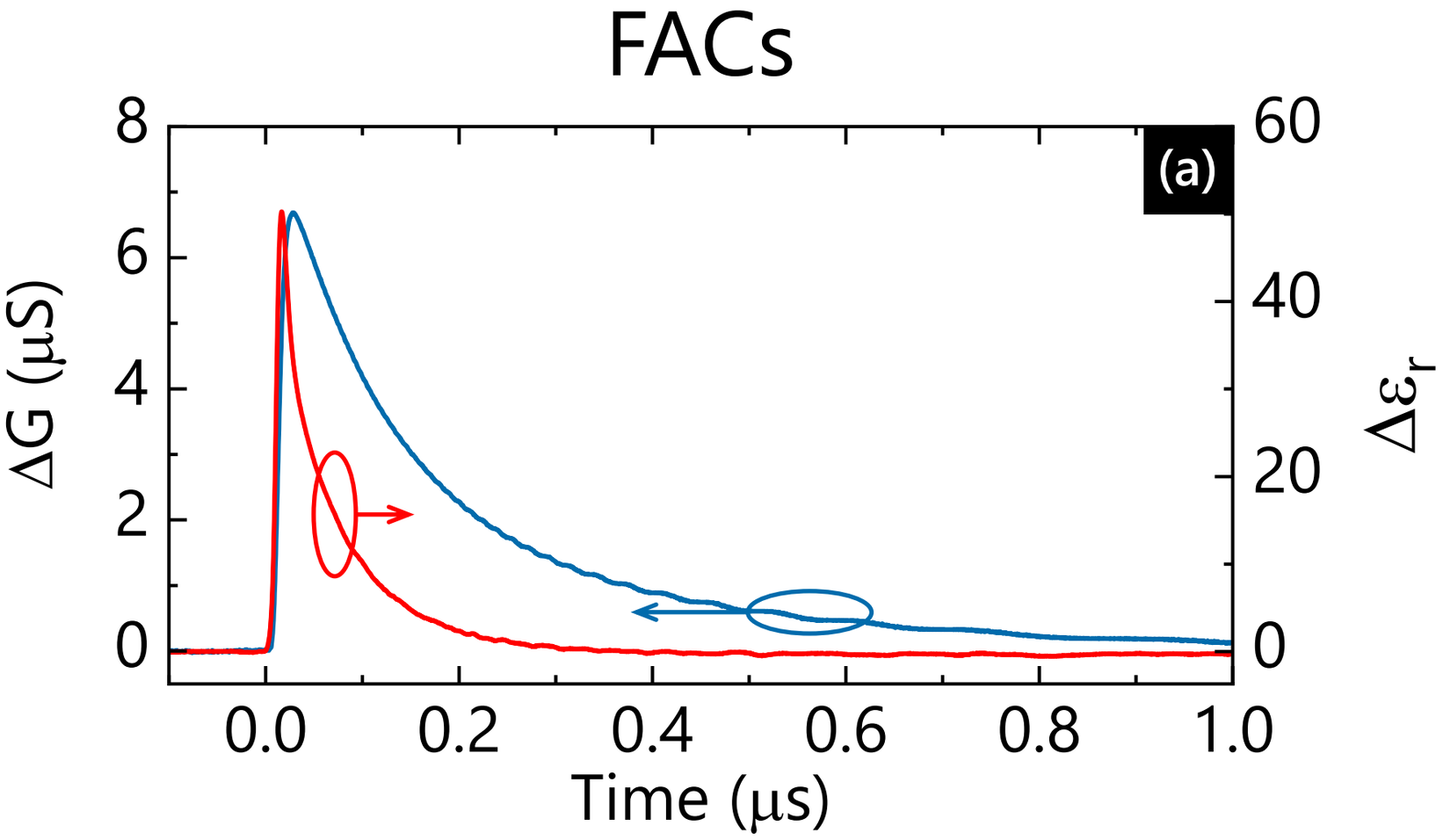
FACs
(a)
ΔG (μS)
Δε_r
Time (μs)
0
2
4
6
8
0
20
40
60
0.0
0.2
0.4
0.6
0.8
1.0

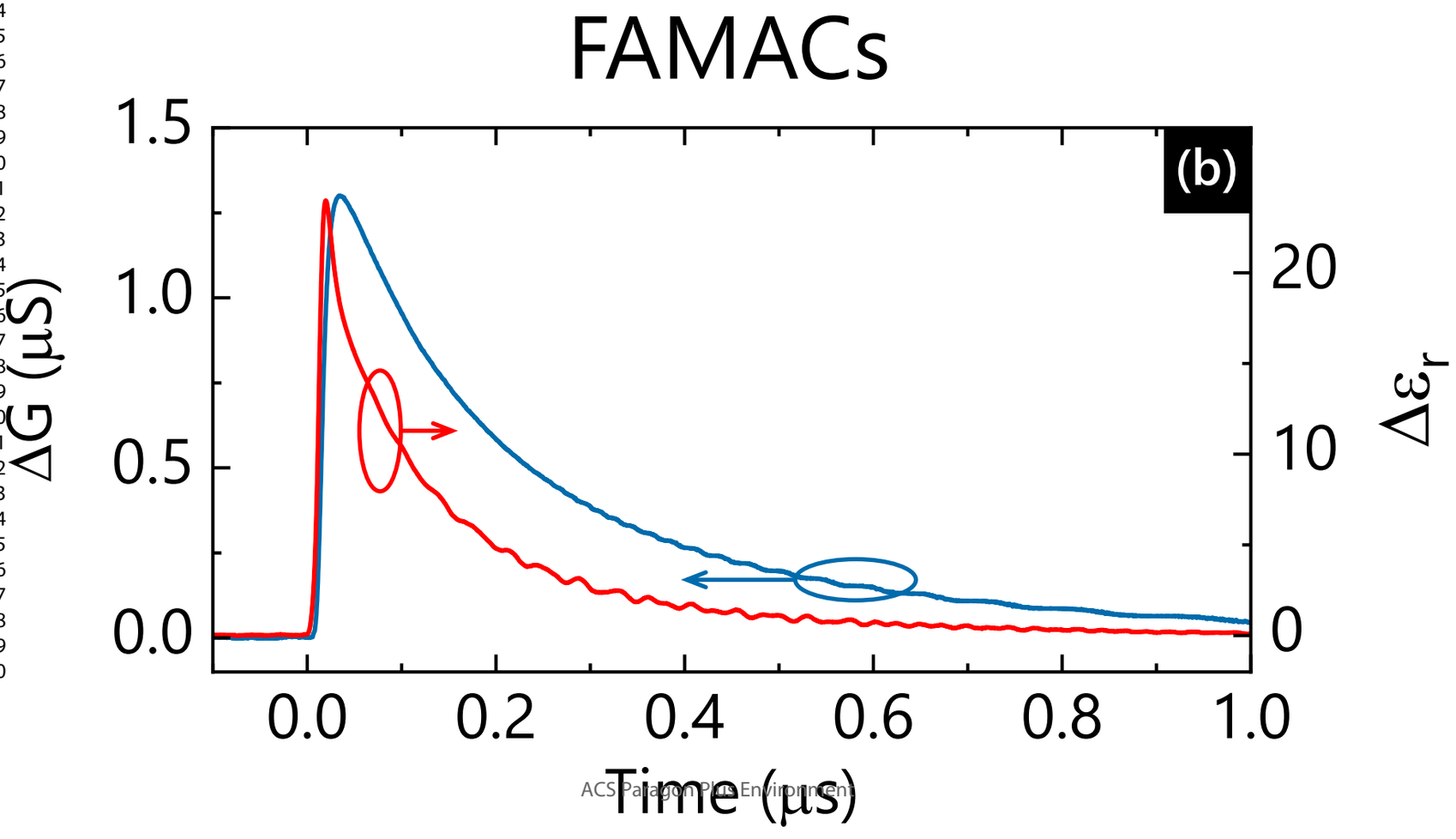
FAMACs
(b)
ΔG (μS)
Δε_r
Time (μs)
0.0
0.5
1.0
1.5
0
10
20
0.0
0.2
0.4
0.6
0.8
1.0

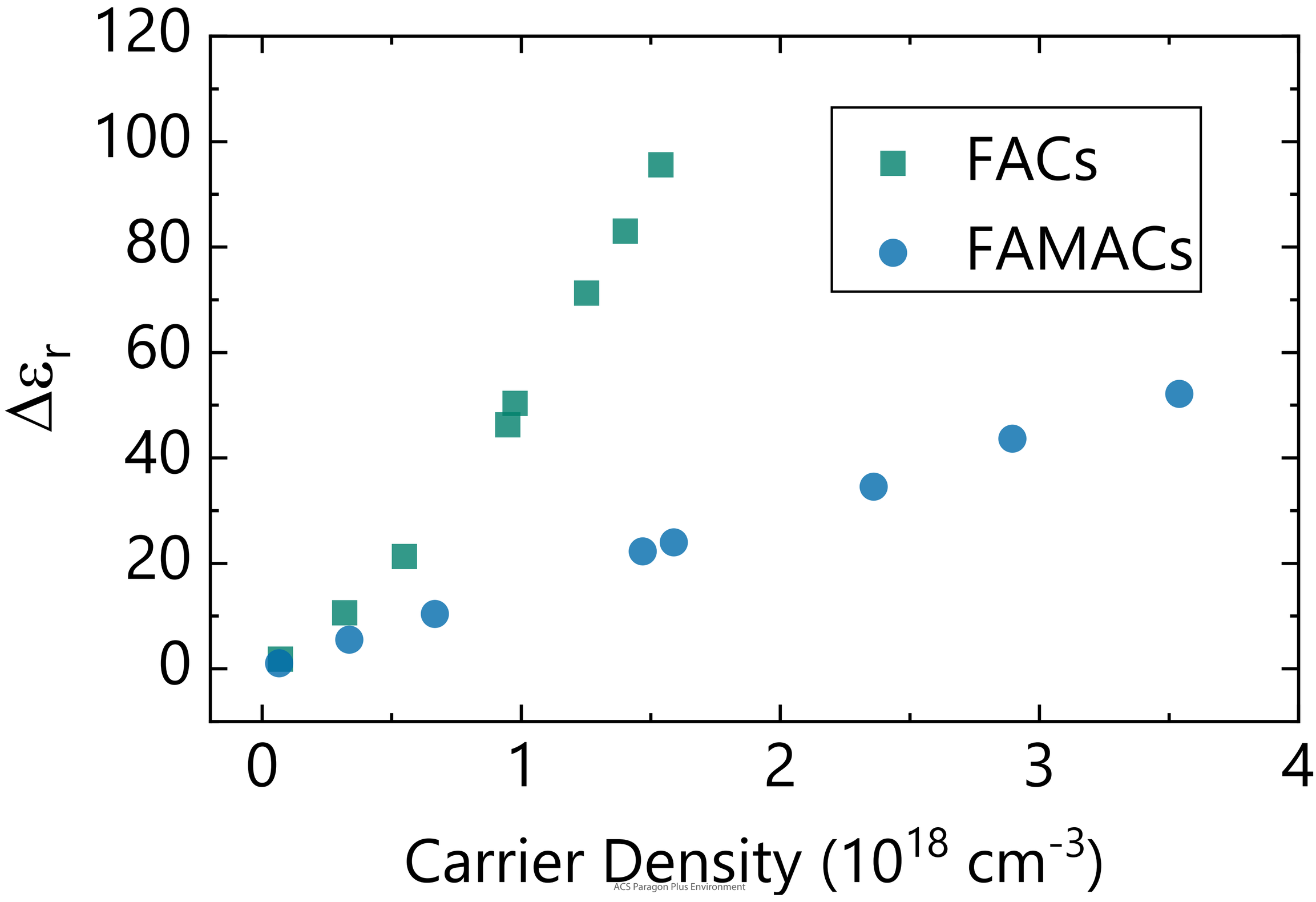
120
100
80
60
40
20
0
$\Delta\varepsilon_r$
0
1
2
3
4
Carrier Density (10^{18} cm^{-3})
FACs
FAMACs

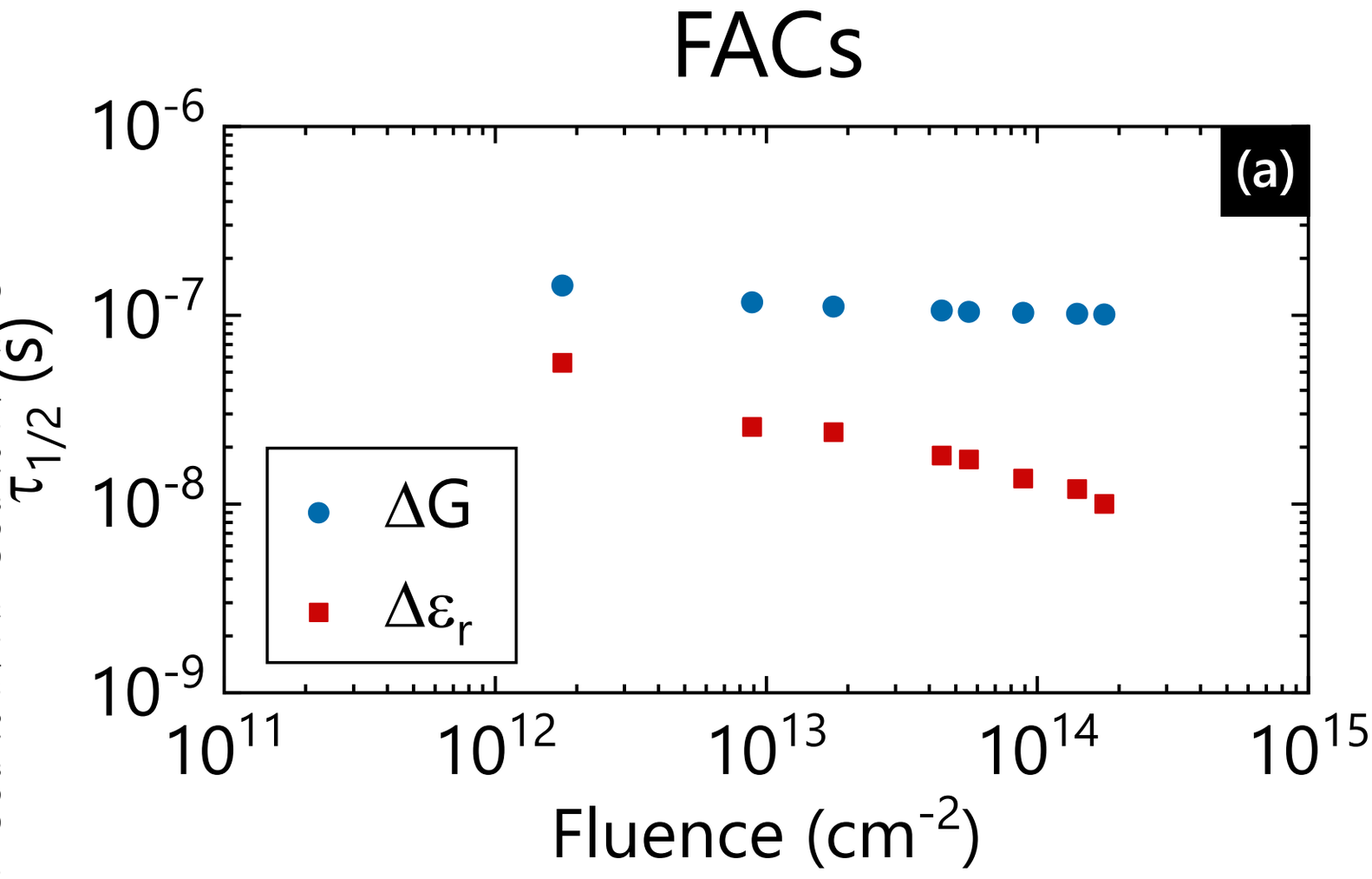
FACs
(a)
10^{-6}
10^{-7}
10^{-8}
10^{-9}
$\tau_{1/2}$ (s)
ΔG
$\Delta\varepsilon_r$
10^{11}
10^{12}
10^{13}
10^{14}
10^{15}
Fluence (cm^{-2})

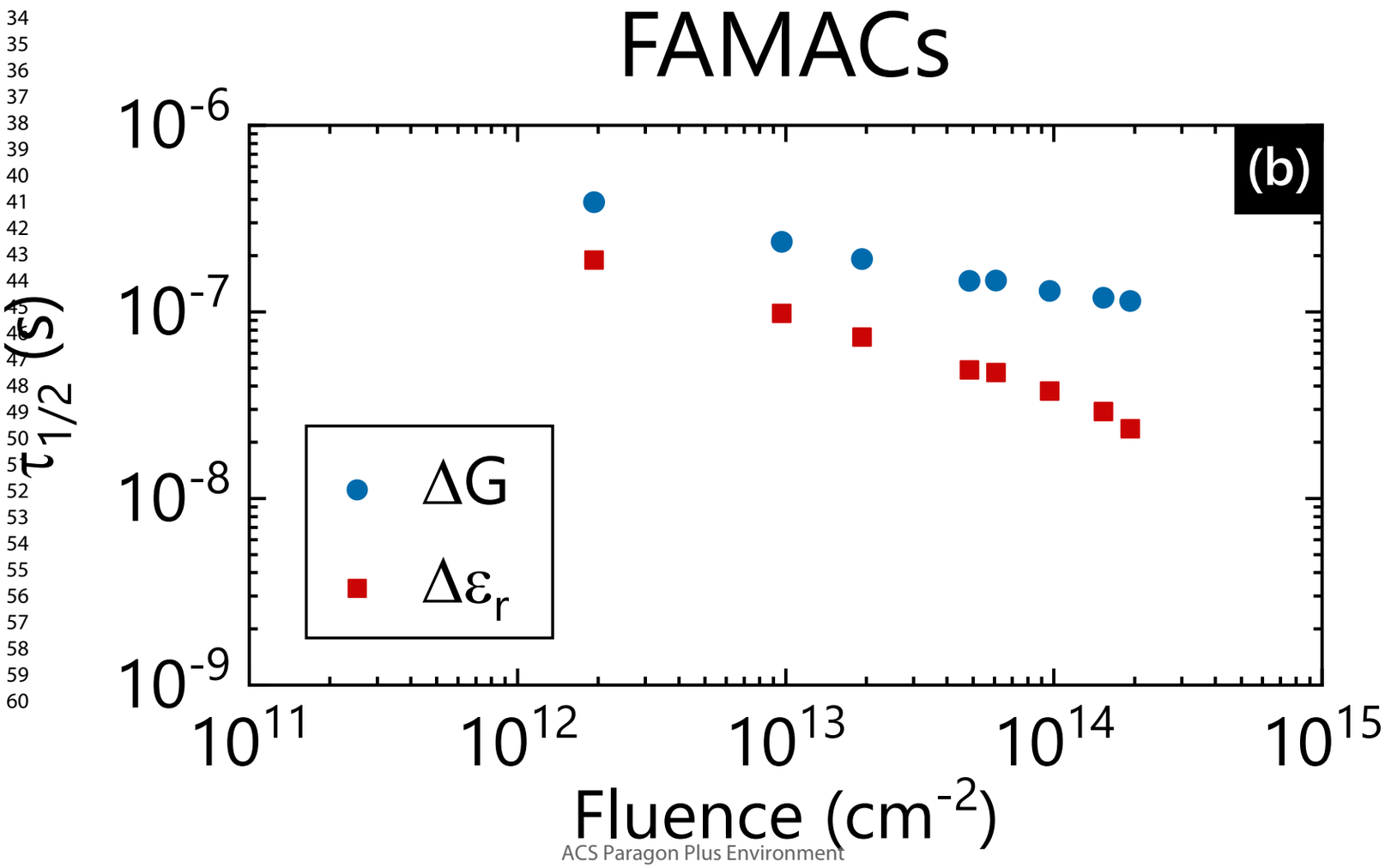
FAMACs
(b)
10^{-6}
10^{-7}
10^{-8}
10^{-9}
$\tau_{1/2}$ (s)
ΔG
$\Delta\varepsilon_r$
10^{11}
10^{12}
10^{13}
10^{14}
10^{15}
Fluence (cm^{-2})

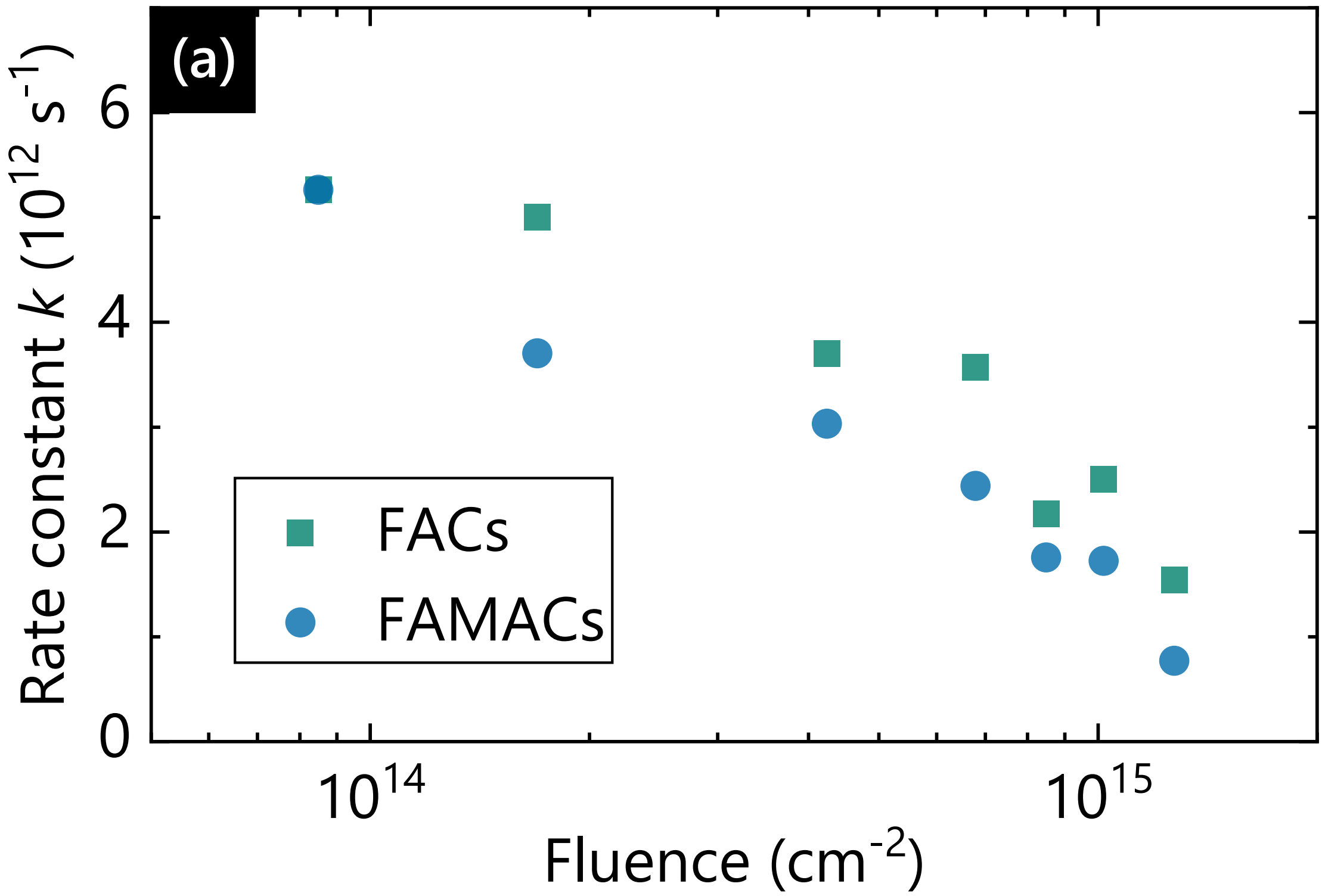
(a)
Rate constant k (10^12 s^-1)
0
2
4
6
10^14
10^15
Fluence (cm^-2)
FACs
FAMACs

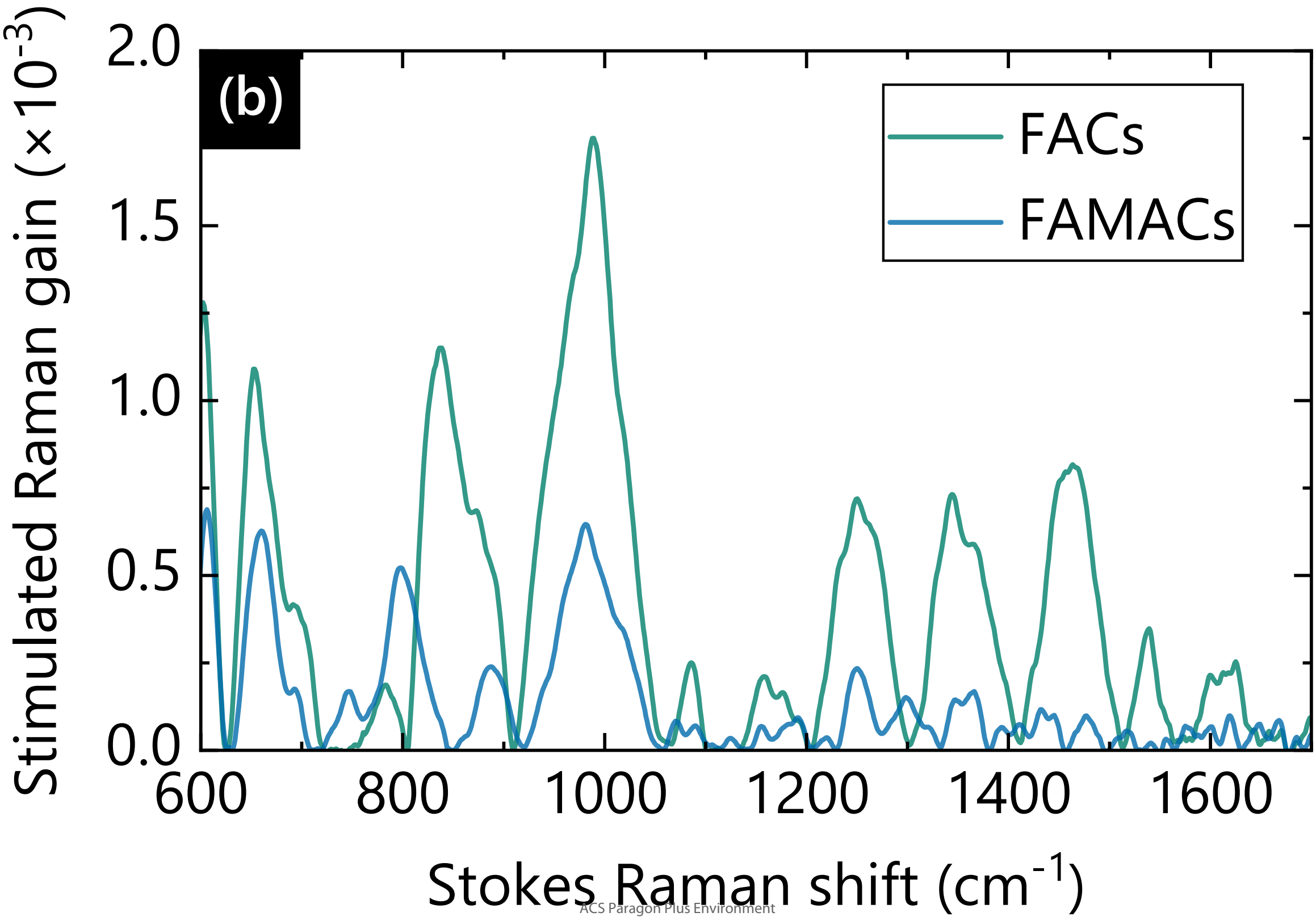
(b)
Stimulated Raman gain (×10^-3)
0.0
0.5
1.0
1.5
2.0
600
800
1000
1200
1400
1600
Stokes Raman shift (cm^-1)
FACs
FAMACs